Journal of Chemical Crystallography (2023) 53:8–15
https://doi.org/10.1007/s10870-022-00955-z

BRIEF COMMUNICATION

Crystal Structure and Hirshfeld Analysis of a Poorly Water Soluble Bis(ligand)copper(II) Complex Containing the Metallophore Pyridine-2-Carboxaldehyde 2-Furoyl Hydrazone

Daphne S. Cukierman[1] · Carolina B. P. Ligiero[2] · Roberto R. de Avillez[3] · Nicolás A. Rey[1]

Received: 16 April 2022 / Accepted: 15 June 2022 / Published online: 25 July 2022

Abstract

The crystal structure of a novel bis(ligand)copper(II) complex of the pyridine-2-carboxaldehyde 2-furoyl hydrazone (HPCFur) metallophore is described, altogether with its Hirshfeld surface analysis. The isolated compound crystallizes in the monoclinic system, space group $P2_1/c$, with four $[Cu(PCFur)_2]$ molecules in the asymmetric unit. Symmetry around copper is distorted octahedral. HPCFur coordinates in its deprotonated, iminolate form, which impacts the O1−C7 and N2−N3 distances in both ligand units. The complex exhibits a variety of weak, non-conventional intermolecular hydrogen bonds. Hirshfeld analysis and fingerprint plots indicate that, overall, hydrogen bond interactions are responsible for almost 50% of the crystal 3D arrangement, while nondirectional H···H contacts account for 38.0%. To the best of our knowledge, this is the first description of a copper(II) complex containing this ligand. The structural characterization of this poorly water soluble species contributes to a better understanding of the intricate equilibria that take place in biologically relevant ternary peptide/protein-copper-hydrazone systems.

Graphical Abstract

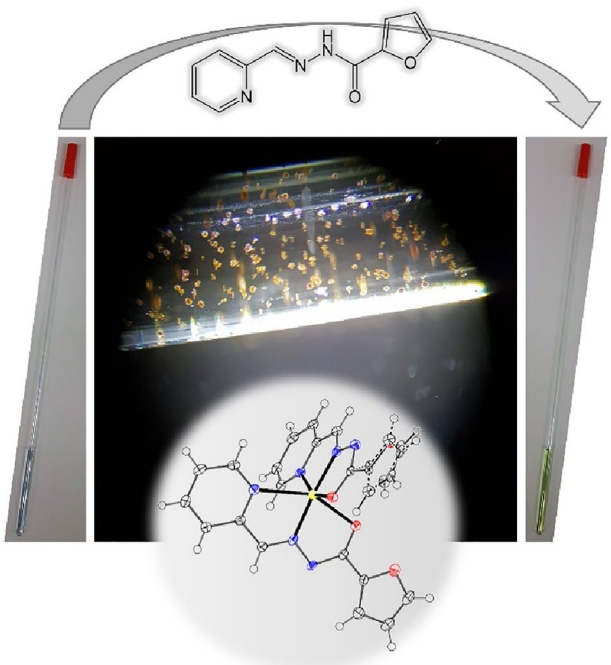

Keywords *N*-acylhydrazones · Copper · Metal complex · XRD · Hirshfeld surface · Fingerprint plots

Extended author information available on the last page of the article

Introduction

During the last decade, attention has been drawn to the use of *N*-acylhydrazones as potential metallophores, or Metal-Protein Attenuating Compounds for the bioinorganic management of neurodegenerative disorders [1]. For example, in our contribution to the special issue "Metals and Degenerative Diseases", published in Journal of Biological Inorganic Chemistry at the end of 2019 [2], we reported on the effect of two pyridine-2-carboxaldehyde-derived *N*-acylhydrazones on the copper-catalyzed oxidation of the M112A $PrP_{103–112}$ mutant fragment (denoted dMKHA). In addition, the paper describes in detail the interaction between copper(II) and the decapeptide at pH 7.4, that occurs through the anchoring site constituted by the side chain of histidine, in a coordination pattern completed by two or three deprotonated amide nitrogens from the main-chain peptide bonds. We employed 1D and 2D NMR spectroscopy not only to propose the coordination sphere of the main species present in equilibrium in the dMKHA–copper(II) system, but also to further study the impact of HPCFur ligand (pyridine-2-carboxaldehyde 2-furoyl hydrazone, Scheme 1) on the peptide interaction with the metal.

During those experiments, we observed the formation of nice amber, geminated crystalline aggregates inside a 3 mm NMR tube (Fig. 1) containing dMKHA peptide, HPCFur *N*-acylhydrazonic ligand and copper(II) at the proportion 1:0.5:0.1. The crystals were formed after the tube was inside the spectrometer for a while during measurements, at a temperature of 5 °C. Unfortunately, single crystals were too small, and their structure could not be elucidated at that time.

More recently, we described in detail a full evaluation of the copper(II) chelation profile of new, HPCFur structure-related, ligands in ternary systems containing a similar, non-mutant, $PrP_{103–112}$ fragment (dMKHM) [3]. Mixed ligand complexes comprising dMKHM, copper(II) ions, and the *N*-acylhydrazone X1Fur were characterized by potentiometry, UV-Vis spectroscopy, and circular dichroism. Some

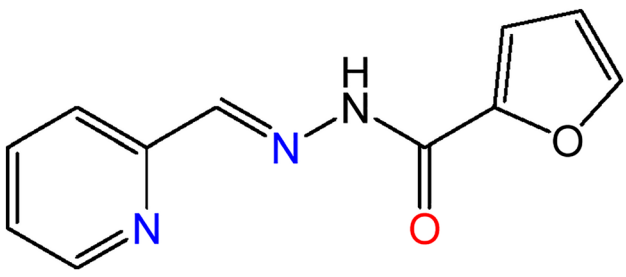

Scheme 1 Chemical structure of the *N*-acylhydrazone HPCFur (pyridine-2-carboxaldehyde 2-furoyl hydrazone). Donor atoms involved in the tridentate coordination are highlighted in color

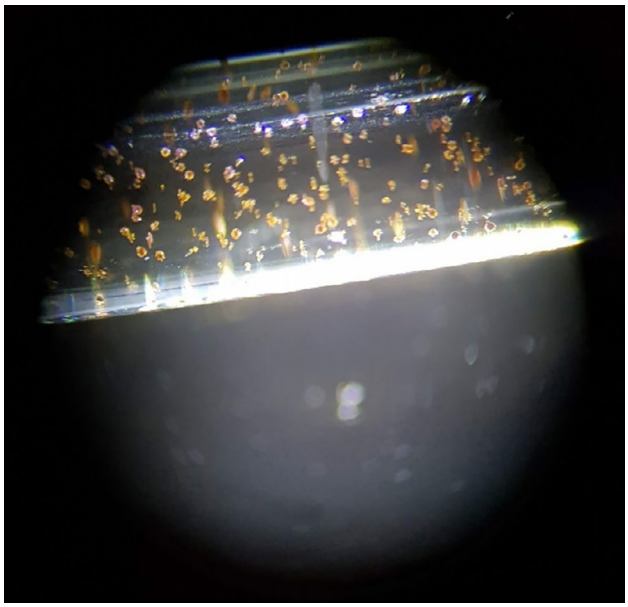

Fig. 1 Single crystals formed inside the NMR tube under optical microscope

species were also identified by ESI-MS and unequivocally assigned through their isotopic distribution pattern. For this kind of three-component systems, we found that, at physiological pH, the ternary peptide-hydrazone-copper complex is the main species and that, in more basic media, bis(hydrazone)copper(II) complex predominates.

In this context, and in order to confirm the nature of this poorly soluble species, and to get additional insights on this type of biologically relevant ternary systems, we managed to crystallize the compound under experimental conditions similar to those employed in the published NMR experiment. Although crystallized at physiological pH, the species showed to be a bis(hydrazone)copper(II) complex (**1**) of the HPCFur ligand. While the structures of copper(I) complexes of HPCFur have been already reported in the literature [4], this is, to the best of our knowledge, the first description of a cupric complex containing this ligand. Therefore, this brief communication reports on the crystal structure of that compound, as well as the respective Hirshfeld surface analysis. The importance of this species for the whole equilibrium panorama in such decapeptide-copper-hydrazone systems is also explored.

Materials and Methods

The decapeptide dMKHA (Ac-SKPKTNMKHA-NH_2) was assembled using the solid-phase peptide synthesis strategy on a Liberty 1 Peptide Synthesizer [5] and kindly

provided by our collaborator Prof. Csilla Kallay (University of Debrecen, Hungary).

To a solution containing dMKHA (5 mmol L^{-1} in 50 mmol L^{-1} HEPES buffer, pH 7.4), 1.2 µL of aqueous 0.55 mol L^{-1} $CuCl_2{\cdot}2H_2O$ was added and the mixture immediately turned blue and turbid. Thus, 100 µL of buffer were added to redissolve the amorphous precipitate. Then, 12.5 µL of HPCFur solution (0.177 mol L^{-1} in methanol) were added to the now clear blue system, which instantly turned yellow. The mixture was reserved protected from light at 4 °C. Single crystals of compound **1** suitable for crystallographic measurements were isolated after some days.

Alternatively, **1** can be synthesized in the absence of peptide by reacting HPCFur (1 mmol) and $CuCl_2{\cdot}2H_2O$ (0.5 mmol) in a 50% water/methanol solvent system. The dark green solid immediately formed was filtered off and discarded, and the filtrate pH, initially at 3, was adjusted to 7 with aqueous NaOH, turning the solution dark yellow. Small crystals of **1** were observed after few hours upon standing at 4 °C. Yield: 39.2 mg (16%). Copper analysis (ICP-OES)—found: 14.3%; calculated for $C_{22}H_{16}O_4N_6Cu$: 12.9%. Mid-infrared spectra of ligand HPCFur and complex **1** were performed in a Perkin-Elmer 100 FT-IR spectrophotometer. Samples were measured as potassium bromide pellets.

Data collection was conducted in a Bruker D8 Venture diffractometer operating at 100 K with Cu Kα (λ = 1.54184 Å, microfocus source, IµS 3.0), and Photon II detector. A total of 1170 images were collected, and 27,579 reflections obtained after integration using a narrow-frame algorithm implemented on Bruker SAINT (V8.40 A) [6]. Absorption was corrected with multi-scan method implemented in SADABS (version 2016/2) [7] on Apex 3 system. Structure was solved with direct methods in ShelxS (version 2013/1) [8] and refined employing full-matrix least-square based on F^2 with ShelxL (version 2018/3), implemented in both WinGX (version 2020.2) [9] and ShelxLE (version QT5-64 rev 1306) [10] softwares. Non-hydrogen atoms were located in Fourier maps and refined anisotropically. Hydrogen atoms were added theoretically and treated by rigid model, with Uiso(H) = 1.2 Ueq. Hirshfeld Surface and Fingerprint Plots were obtained with Crystal Explorer (version 17.5) [11]. Other figures and analyses were created with Mercury (version 2021.2.0) [12] and Platon (21/12/20) programs [13].

The powder XRD pattern was obtained on a Bruker D8 Discover diffractometer operating at 40 kV and 40 mA, using Cu Kα radiation, Ni filter, LynxEye detector, and Bragg-Brentano geometry. A background-free sapphire sample holder was employed to collect the diffraction between 5° and 40° (2θ), step size of 0.02°. Acquisition time was adjusted to obtain a minimum of 25,000 counts on the most intense peak. Rietveld fitting with fundamental parameters were done using Profex 5.0 [14] and Topas [15] softwares.

Results and Discussion

The isolated compound crystallizes in the monoclinic system, space group $P2_1/c$, with four $[Cu(PCFur)_2]$ molecules in the asymmetric unit. Crystal, data collection and refinement parameters are summarized in Table 1. The corresponding ORTEP view is shown in Fig. 2. Selected bond distances and angles are given in Table 2.

Symmetry around copper is distorted octahedral. The ligand coordinates in its deprotonated, iminolate form, which impacts the O1−C7 and N2−N3 distances in both HPCFur units. This *N*-acylhydrazone (NAH), as expected, performs like a tridentate, meridional ligand through the pyridine and azomethine nitrogen atoms and the iminolate oxygen. As a consequence of this coordination mode, combined with the pronounced Jahn-Teller effect displayed by copper(II), the ligand units are not equivalent and one of them (unit A), occupying the equatorial plane of the molecule, is more tightly bound to the metal center than the other (unit B), which lies along the elongated *z*-axis. This so-called axial ligand is much more prone to protonation at the N3 atom than the equatorial one, which explains the presence of the $[Cu(NAH_{protonated})(NAH_{deprotonated})]^+$ species in the equilibrium models proposed for the related systems containing the hydrazones X1Fur and X1Thio [3]. The structure of **1** is similar to other structures previously published in the literature, such as the one of $[Cu(PCIH)_2]$

Table 1 Crystal data, collection, and refinement parameters for **1**

Chemical formula	$C_{22}H_{16}O_4N_6Cu$
Formula weight (g mol^{-1})	491.95
Crystal system	Monoclinic
Space group	$P2_1/c$
Temperature (K)	100(2)
a, b, c (Å)	10.9421(12), 8.3376(10), 22.303(3)
β (°)	93.804(5)
Z	4
Cell volume ($Å^3$)	2030.2(4)
F (000)	1004
µ (mm^{-1})	1.914
Cystal size (mm)	0.358 × 0.126 × 0.050
T_{min}, T_{max}	0.5906, 0.7536
h,k,l (min; max)	− 13; 13; − 9; 10; − 27; 27
R_{int}	0.0799
Theta Min, Max	3.973, 67.679
$R[F^2 > 2\sigma(F^2)]$, $wR(F^2)$, S	0.0487, 0.1137, 1.005
Reflections/Parameters	3843 /314
No. of restrains	6
$\Delta\rho_{max}$, $\Delta\rho_{min}$ (e $Å^{-3}$)	− 0.67, 0.55
Data completeness	0.961

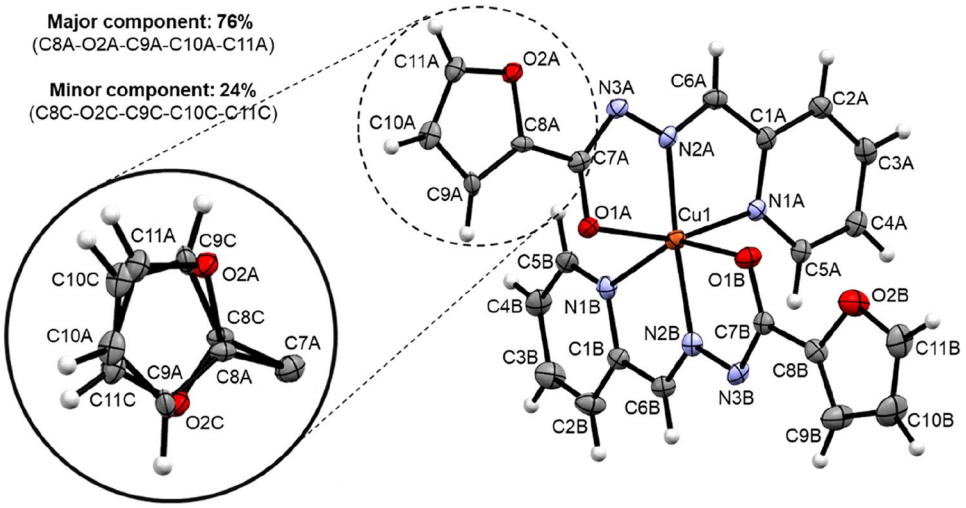

Fig. 2 ORTEP representation of the crystal structure of **1**. The disorder in the equatorial furoyl ring is highlighted. Ellipsoids were drawn with 50% probability level

Table 2 Selected bond distances and angles for **1**

Bond distances (Å)		Bond angles (°)	
Cu1–O1A	2.0467(18)	O1A–Cu1–O1B	92.70(8)
Cu1–O1B	2.260(2)	O1A–Cu1–N1A	157.38(9)
Cu1–N1A	2.062(2)	O1A–Cu1–N1B	93.40(8)
Cu1–N1B	2.462(3)	O1A–Cu1–N2A	78.20(9)
Cu1–N2A	1.943(2)	O1A–Cu1–N2B	103.27(9)
Cu1–N2B	1.981(2)	O1B–Cu1–N1A	94.49(9)
O1A–C7A	1.273(4)	O1B–Cu1–N1B	150.03(8)
O1B–C7B	1.261(4)	O1B–Cu1–N2A	98.70(9)
N2A–N3A	1.366(3)	O1B–Cu1–N2B	75.45(9)
N2B–N3B	1.378(3)	N1A–Cu1–N1B	91.02(9)
		N1A–Cu1–N2A	79.52(10)
		N1A–Cu1–N2B	99.29(10)
		N1B–Cu1–N2A	111.28(9)
		N1B–Cu1–N2B	74.59(9)
		N2A–Cu1–N2B	173.97(10)

[16]. It is worth noting that, in spite of their similarity, the first $PCFur^-$ unit, occupying equatorial coordination sites, binds copper(II) in a stronger way than $PCIH^-$, given its shorter N1A−Cu1 and O1A−Cu1 distances [2.062(2) vs. 2.118(3) Å and 2.0467(18) vs. 2.096(3) Å, respectively]. On the other hand, the axial $PCFur^-$ pyridine nitrogen N1B is much weaklier bound than the corresponding atom of $PCIH^-$ [2.462(3) vs. 2.301(4) Å]. A broader comparison involving analogous structures from CSD database (CSD 5.42, sep21 update) performed using the software Mogul 2021.2.0 [17] showed that most geometrical parameters in **1** are close to those found in similar structures. An exception is precisely the Cu1–N1B distance, the longest among 173 related copper complexes. The average Cu–N distance is 2.093(96) Å.

Another interesting aspect in this structure is the positional disorder observed in the equatorial furoyl ring. A two-site model was employed (detail in Fig. 2). Major component A (76%) has the oxygen pointing out, while in the minor component C (24%) oxygen is pointing in, although in both cases the ring is near coplanar with the molecular structure. Axial ligand (B-coded) does not exhibit such disorder.

Complex **1** exhibits a variety of weak, non-conventional intermolecular hydrogen bonds. A pair of such interactions involving O1B as acceptor (namely, C10A*−H···O1B and O1B··· H−C11B**) give origin to a tape motif that grows along crystallographic axis *b* (Fig. 3A). The arrangement is also mediated by polar π···π stacking contacts involving pyridine and furan rings, slipped by 1.467 Å, of A-coded equatorial ligands from different molecules of **1**. Distance between centroids is 3.599(5) Å and between π-planes is 3.286(5) Å. The relatively strong nature of this interaction is evidenced by the d_{norm} Hirshfeld surface displayed in Fig. 3B. The zigzag chains thus generated interact with each other through cross C5A−H···N3B*** bonds (not shown). Table 3 summarizes the whole landscape of hydrogen bonds present in the crystal lattice of **1**.

The d_{norm} Hirshfeld representations display, in the form of red spots, the portions over the molecule surface where the distance from the nearest atom of the neighboring molecule is smaller than the respective van der Waals radii sum, thus highlighting the strongest interactions. Figure 3C reveals that the main intermolecular connections are those involving nondirectional H···H contacts, followed by non-conventional CH···O and CH···N bonds, CH···π and π···π interactions. Fingerprint plots confirm this result, showing CH···O hydrogen bonds (21.4%) as well-defined spikes, CH···N (10.9%) as less pronounced spikes and CH···π (17.3%) typically as wing-shaped regions. On the other hand, the π···π contact can be observed as a light-blue area at the center of the map. Overall, hydrogen bond interactions are responsible for

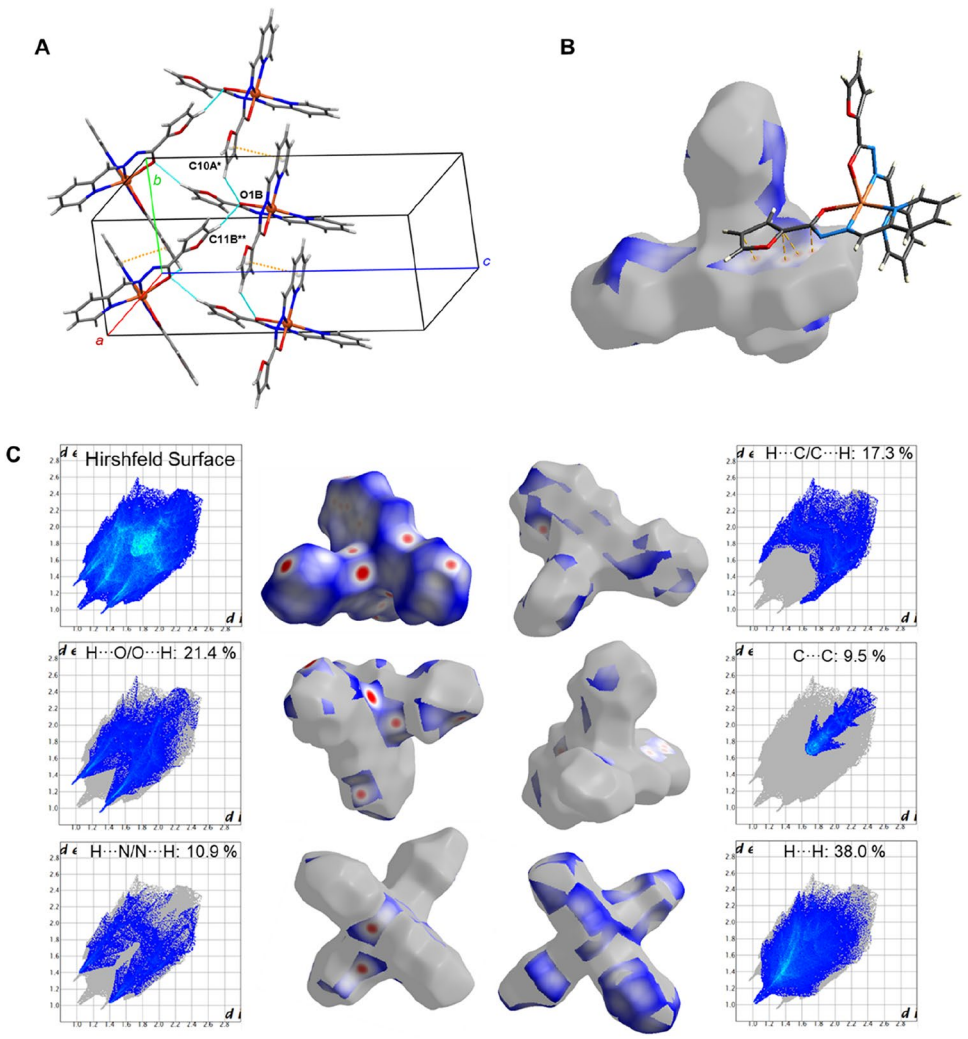

Fig. 3 Intermolecular interactions observed in the crystal lattice of **1**. **A** Non-conventional hydrogen bonds (light blue lines) generate a zig-zag tape motif running parallel to the crystallographic axis *b*, which is further stabilized by π···π stacking contacts (orange dotted lines). **B** Analysis of the Hirshfeld surface mapped with d_{norm} (– 0212 to 1.016), and filtered by C···C interactions, confirm the relatively strong nature of the π···π stacking contacts. **C** Fingerprint plots indicate that the main interactions present are, in decreasing order, non-conventional CH···O and CH···N bonds, as well as CH···π and π···π contacts (Color figure online)

Table 3 Hydrogen bond geometric parameters for complex **1**

D–H···A	D–H (Å)	H···A (Å)	D···A (Å)	D–H···A (°)
C10A*–H···O1B	0.9500	2.5900	3.167(8)	120.00
O1B···H–C11B**	0.9500	2.3600	3.287(4)	164.00
C5A–H···N3B***	0.9500	2.5100	3.204(4)	130.00

Symmetry codes: *x, $1+y$, z , **$1-x$, $-½+y$, $½-z$, ***$1-x$, $2-y$, $1-z$

almost 50% of the Hirshfeld surface, while nondirectional H···H contacts account for 38.0%.

Relevance of the crystallographic findings to the equilibrium panorama involving this kind of three-component systems: while **1** was obtained in the presence of dMKHA, the decapeptide did not take part in the crystal lattice, confirming the results previously reported by us on the effective disruption of peptide-copper(II) interactions by tridentate *N*-acylhydrazones, when in excess from 3-fold on [3, 18–20]. In fact, simulations performed through the Hyss

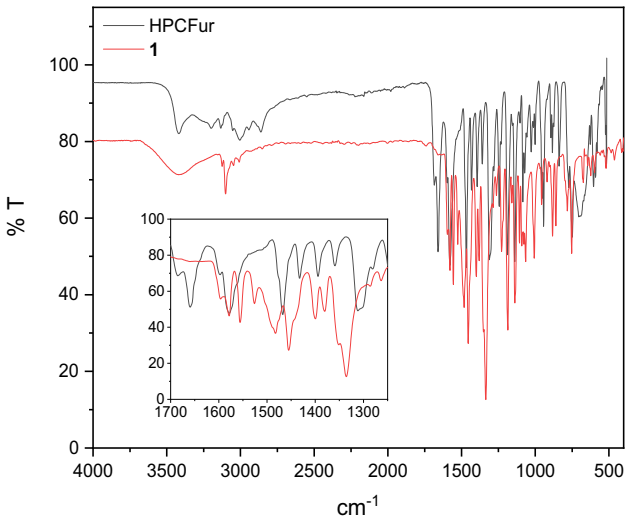

Fig. 4 Mid-infrared spectrum of HPCFur and complex **1** (KBr). *Inset*: magnification of the 1700–1250 cm^{-1} region

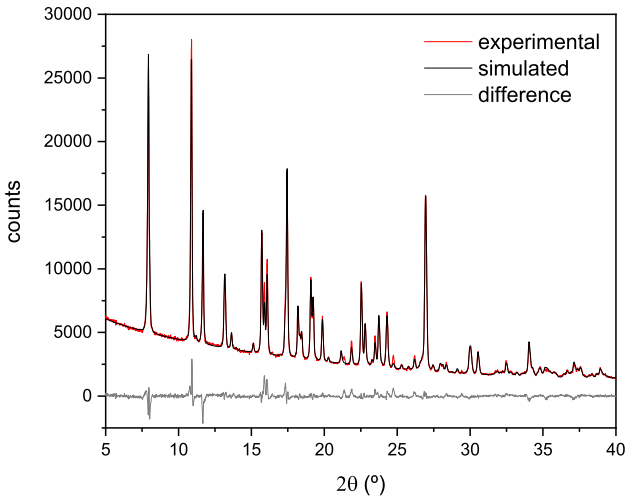

Fig. 5 Comparison, at the small angle limit, between the experimental diffractogram of **1** (synthesized in the absence of peptide) and that simulated from the monocrystal .cif file. Difference is also included

2009 program [21] for a system containing the closely related X1Fur ligand indicate that, under the conditions used in the crystallization of **1**, metal-containing species predominating at pH 7.4 are the partially protonated and the fully deprotonated bis(hydrazone) complexes. In such an excess of ligand, the ternary peptide-copper-NAH species is minoritarian. As **1** is the only neutral species, it precipitates from the solution. This was not observed for the complex derived from the 1-methylimidazole-containing ligand X1Fur, due to its higher water solubility.

Nevertheless, complex **1** can also be prepared through more direct protocols as well. The one reported in the present work involved the reaction between two equivalents of HPCFur and one of copper(II) chloride, with initial precipitation of an ML complex. After filtration and pH neutralization, complex **1** was isolated as a polycrystalline solid upon cooling. The small yield obtained is probably related to the loss of reactant mass in the form of the monoligand coordination compound ML. Figure 4 displays the overlapped infrared spectra of HPCFur and complex **1**. Most of the ligand bands are still observed in the spectrum of **1**, although some specific frequencies shifts constitute unequivocal signs of the hydrazone deprotonation and coordination to copper.

In order to check if the crystalline phase of **1** samples synthesized in the presence and the absence of dMKHA were the same, we performed a powder XRD study in which the experimental diffraction pattern of the sample prepared in the absence of the peptide was compared to the pattern simulated from the monocrystal .cif file (Fig. 5). As it can be concluded by the difference between them (gray line in the figure), both diffractograms are fully consistent. The lattice parameters obtained were $a = 11.0507(4)$, $b = 8.4435(4)$, $c = 22.354(1)$ Å, and $\beta = 94.015(3)°$ and the fitting quality parameters were $R_{wp} = 4.42$, $R_p = 3.03$, and gof = 2.68, confirming the excellent overall fitting. Nonetheless, three small peaks at 16.45°, 21.32°, and 29.43° 2θ values were not fitted, which may be related to the presence of some very small unidentified crystalline impurity. The powder showed a preferred orientation consistent with the observed needle morphology, that was adjusted with spherical harmonics. The mean crystallite size, modeled with a Lorentzian curve and determined by the integral breadth [22], was equal to 163 ± 6 nm.

Conclusions

In spite of the existence of some reports about bis(aroylhydrazone)copper(II) complexes in the literature, the novelty of the present work resides on the fact that **1** was obtained in the presence of a coordinating decapeptide, a mutant fragment of the human prion protein. This constitutes another clear experimental evidence of *N*-acylhydrazone metal abstraction from the protein, an important mechanism of action for metallophores proposed for the management of metal-enhanced aggregopathies such as Alzheimer's, Parkinson's and Transmissible Spongiform Encephalopathies.

Hirshfeld surfaces and fingerprint plots were employed to visualize and better characterize the intermolecular interactions in the crystal lattice. The analysis indicated the presence of intermolecular connections involving nondirectional H···H contacts, non-conventional CH···O and CH···N bonds, as well as CH···π and π···π interactions.

Complex **1** can alternatively be prepared in the absence of dMKHA. Powder XRD patterns demonstrated that both samples have the same crystalline phase, regardless of the methodology employed for their synthesis.

The structural characterization of this poorly water soluble species contributes to a better understanding of the intricate equilibria that take place in biologically relevant ternary peptide/protein-copper-hydrazone systems.

Acknowledgements All authors are grateful to the scientific Brazilian agency CNPq (Conselho Nacional de Desenvolvimento Científico e Tecnológico) for the research fellowships and scholarship awarded. NAR is also grateful to FAPERJ (Fundação Carlos Chagas Filho de Amparo à Pesquisa do Estado do Rio de Janeiro) for the "Cientista do Nosso Estado" fellowship granted. We would like to acknowledge Ministério da Ciência e Tecnologia (MCT) and Financiadora de Estudos e Projetos (FINEP)—Grant # Convênio: 01.11.0100.00. We thank Centro Nacional de Biologia Estrutural e Bioimagem (CENABIO) for the support with the X-ray diffraction facility (D8-Venture). The authors are also thankful to Prof. Csilla Kallay, for providing the decapeptide. CBPL acknowledges the Brazilian Chemical Society and Royal Society of Chemistry for the prize "Young Researcher of Royal Society of Chemistry—RASBQ 2021".

Author Contributions DSC and NAR conceived the experiments, interpreted the data, and wrote the paper. DSC also performed the

syntheses of **1**. CBPL and RRA performed the XRD measurements, structure refinement and analyses, and wrote the paper for the crystallography part.

Data Availability CCDC 2176002 contains the supplementary crystallographic data for **1**. These data can be obtained free of charge *via* www.ccdc.cam.ac.uk/data_request/cif, or by emailing data_request@ccdc.cam.ac.uk, or by contacting Cambridge Crystallographic Data Centre, 12 Union Road, Cambridge CB2 1EZ, UK; fax: +44 1223 336,033.

Declarations

Conflict of interest The authors declare no conflict of interest.

References

1. Cukierman DS, Rey NA (2022) Tridentate N-acylhydrazones as moderate ligands for the potential management of cognitive decline associated with metal-enhanced neuroaggregopathies. Front Neurol. https://doi.org/10.3389/fneur.2022.828654
2. Cukierman DS, Bodnár N, Evangelista BN, Nagy L, Kállay C, Rey NA (2019) Impact of pyridine-2-carboxaldehyde-derived aroylhydrazones on the copper-catalyzed oxidation of the M112A PrP. J Biol Inorg Chem 24:1231–1244. https://doi.org/10.1007/s00775-019-01700-2
3. Cukierman DS, Bodnár N, Diniz R, Nagy L, Kállay C, Rey NA (2022) Full equilibrium picture in aqueous binary and ternary systems involving copper(II), 1-methylimidazole-containing hydrazonic ligands, and the 103–112 human prion protein fragment. Inorg Chem 61:723–737
4. Gholivand K, Farshadfar K, Roe SM, Hosseini M, Gholami A (2016) Investigation of structure-directing interactions within copper(i) thiocyanate complexes through X-ray analyses and non-covalent interaction (NCI) theoretical approach. CrystEngComm 18:7104–7115
5. Csire G, Nagy L, Várnagy K, Kállay C (2017) Copper(II) interaction with the human prion 103–112 fragment—coordination and oxidation. J Inorg Biochem 170:195–201. https://doi.org/10.1016/j.jinorgbio.2017.02.018
6. Bruker Apex-III (2012). In: Inc BA (ed) Madison, Wisconsin, USA
7. Krause L, Herbst-Irmer R, Sheldrick GM, Stalke D (2015) Comparison of silver and molybdenum microfocus X-ray sources for single-crystal structure determination. J Appl Crystallogr 48:3–10. https://doi.org/10.1107/S1600576714022985
8. Sheldrick GM (2008) A short history of SHELX. Acta Crystallogr A 64:112–122. https://doi.org/10.1107/S0108767307043930
9. Farrugia LJ (2012) WinGX and ORTEP for windows: an update. J Appl Crystallogr 45:849–854
10. Hubschle CB, Sheldrick GM, Dittrich B (2011) ShelXle: a Qt graphical user interface for SHELXL. J Appl Crystallogr 44:1281–1284. https://doi.org/10.1107/S0021889811043202
11. Spackman PR, Turner MJ, McKinnon JJ, Wolff SK, Grimwood DJ, Jayatilaka D, Spackman MA (2021) CrystalExplorer: a program for Hirshfeld surface analysis, visualization and quantitative analysis of molecular crystals. J Appl Crystallogr 54:1006–1011. https://doi.org/10.1107/S1600576721002910
12. Macrae CF, Edgington PR, McCabe P, Pidcock E, Shields GP, Taylor R, Towler M, van de Streek J (2006) Mercury: visualization and analysis of crystal structures. J Appl Crystallogr 39:453–457. https://doi.org/10.1107/S002188980600731X
13. Spek A (2009) Structure validation in chemical crystallography. Acta Crystallogr D 65:148–155. https://doi.org/10.1107/S090744490804362X
14. Doebelin N, Kleeberg R (2015) Profex: a graphical user interface for the Rietveld refinement program. J Appl Crystallogr 48:1573–1580. https://doi.org/10.1107/S1600576715014685
15. Coelho A (2018) TOPAS and TOPAS-academic: an optimization program integrating computer algebra and crystallographic objects written in C++. J Appl Crystallogr 51:210–218. https://doi.org/10.1107/S1600576718000183
16. Armstrong CM, Bernhardt PV, Chin P, Richardson DR (2003) Structural variations and formation constants of first-row transition metal complexes of biologically active aroylhydrazones. Eur J Inorg Chem 2003:1145–1156
17. Bruno IJ, Cole JC, Edgington PR, Kessler M, Macrae CF, McCabe P, Pearson J, Taylor R (2002) New software for searching the Cambridge Structural Database and visualizing crystal structures. Acta Crystallogr B 58:389–397. https://doi.org/10.1107/s0108768102003324
18. Hauser-Davis RA, de Freitas LV, Cukierman DS, Cruz WS, Miotto MC, Landeira-Fernandez J, Valiente-Gabioud AA, Fernández CO, Rey NA (2015) Disruption of zinc and copper interactions with Aβ(1–40) by a non-toxic, isoniazid-derived, hydrazone: a novel biometal homeostasis restoring agent in Alzheimer's disease therapy? Metallomics 7:743–747. https://doi.org/10.1039/c5mt00003c
19. Cukierman DS, Pinheiro AB, Castiñeiras-Filho SL, da Silva AS, Miotto MC, De Falco A, de Ribeiro T, Maisonette S, da Cunha AL, Hauser-Davis RA, Landeira-Fernandez J, Aucélio RQ, Outeiro TF, Pereira MD, Fernández CO, Rey NA (2017) A moderate metal-binding hydrazone meets the criteria for a bioinorganic approach towards Parkinson's disease: therapeutic potential, blood-brain barrier crossing evaluation and preliminary toxicological studies. J Inorg Biochem 170:160–168. https://doi.org/10.1016/j.jinorgbio.2017.02.020
20. Cukierman DS, Lázaro DF, Sacco P, Ferreira PR, Diniz R, Fernández CO, Outeiro TF, Rey NA (2020) X1INH, an improved next-generation affinity-optimized hydrazonic ligand, attenuates abnormal copper(I)/copper(II)-α-Syn interactions and affects protein aggregation in a cellular model of synucleinopathy. Dalton Trans 49:16252–16267. https://doi.org/10.1039/d0dt01138j
21. Alderighi L, Gans P, Ienco A, Peters D, Sabatini A, Vacca A (1999) Hyperquad simulation and speciation (HySS): a utility program for the investigation of equilibria involving soluble and partially soluble species. Coord Chem Rev 184:311–318
22. Scardi P, Leoni M, Delhez R (2004) Line broadening analysis using integral breadth methods: a critical review. J Appl Crystallogr 37:381–390. https://doi.org/10.1107/S0021889804004583

Authors and Affiliations

Daphne S. Cukierman[1] · Carolina B. P. Ligiero[2] · Roberto R. de Avillez[3] · Nicolás A. Rey[1]

✉ Daphne S. Cukierman
daphcukierman@gmail.com

✉ Nicolás A. Rey
nicoarey@puc-rio.br

[1] Departamento de Química, Pontifícia Universidade Católica do Rio de Janeiro, Marquês de São Vicente, 225, Rio de Janeiro, RJ 22451-900, Brazil

[2] Departamento de Química Inorgânica, Universidade Federal Fluminense, Campus do Valonguinho, Outeiro de São João Batista, s/n, Niterói, RJ 24020-141, Brazil

[3] Departamento de Engenharia Química e de Materiais, Pontifícia Universidade Católica do Rio de Janeiro, Marquês de São Vicente, 225, Rio de Janeiro, RJ 22451-900, Brazil